

To appear in the Astrophysical Journal

Discovery of an Extended Dust Emission around IRAS 18576+0341 (AFGL 2298) at 10.3 and 18.0 microns: a New Luminous Blue Variable Candidate?

Toshiya Ueta and Margaret Meixner

Department of Astronomy, MC-221, University of Illinois at Urbana-Champaign, Urbana, IL 61801, ueta@astro.uiuc.edu, meixner@astro.uiuc.edu

Aditya Dayal

IPAC/JPL, Caltech, MS 100-22, 770 South Wilson Ave. Pasadena, CA 91125, adayal@ipac.caltech.edu

Lynne K. Deutsch

Department of Astronomy/CAS 519, Boston University, 725 Commonwealth Avenue, Boston, MA 02215, deutschl@bu.edu

Giovanni Fazio and Joseph L. Hora

Harvard-Smithsonian Center for Astrophysics, MS 65, 60 Garden St., Cambridge, MA 02138, jhora@cfa.harvard.edu, gfazio@cfa.harvard.edu

William F. Hoffmann

Steward Observatory, University of Arizona, Tucson, AZ 85721, whoffmann@as.arizona.edu

ABSTRACT

We report detection of an extended mid-infrared emission from IRAS 18576+0341 (AFGL 2298). The object shows a dusty circumstellar shell that has diameter of $\gtrsim 7''$ at 10.3 and 18.0 μm . The dust nebula shows two emission peaks concentrically elongated and symmetrically oriented on the opposite sides of the third, central peak, which appears to be the central star of the system. The observed mid-infrared morphology indicates that the circumstellar dust shell has an equatorially-enhanced material distribution, which is a common signature of stellar objects that have experienced mass loss. Radiative transfer model calculations suggest that the central star is an extremely bright ($L_* = 10^{6.4} L_\odot$) star at a distance of about 10 kpc: this object is best described as a new luminous blue variable candidate. The circumstellar dust shell seems to have been generated by an equatorially-enhanced mass loss process with $\dot{M} \geq 6.8 \times 10^{-6} M_\odot \text{ yr}^{-1}$ and $\dot{M}_{\text{pole}}/\dot{M}_{\text{eq}} \sim 0.5$.

Subject headings: circumstellar matter — dust, extinction — infrared: stars — stars: mass loss — stars: individual (IRAS 18576+0341) — stars: individual (AFGL 2298)

1. Introduction

Mid-infrared (mid-IR; $8 - 25\mu m$) imaging provides powerful means to directly probe the distribution of circumstellar matter, especially circumstellar dust grains. High-resolution ($\sim 1''$) mid-IR images can reveal the structure at the innermost regions of the circumstellar dust shells (CDSs), because the emission is generally optically thin and arises from the warmest ($100 - 200$ K) dust grains in the CDSs. Such mid-IR images of the CDSs have shown that many stars have lost or have been losing their mass in an equatorially-enhanced manner, resulting in toroidal or ring shaped CDSs. For example, the axisymmetric shaping of planetary nebulae is considered to be initiated by an equatorially-enhanced dust-driven wind mass loss at the end of the asymptotic giant branch phase (e.g., Ueta, Meixner, & Bobrowsky 2000 and references therein). The axisymmetric morphologies of the nebulae around luminous blue variables (LBVs) are explained similarly by the presence of an equatorially-enhanced CDS (Nota et al. 1995), which may be generated by stellar rotation near the Eddington limit (Langer, García-Segura, & Mac Low 1999) or the tidal action of the central binary system (Damineli et al. 2000).

In this paper, we report our discovery of an extended dust shell around an unidentified IR object, *IRAS* 18576+0341 (*IRAS* 18576, hereafter), during our observing run to obtain high-resolution mid-IR images of CDSs around evolved stars. After reviewing previous observations in §2, we present the observed images in §3. The results of the dust radiative transfer model calculations are presented in §4, followed by a discussion on the nature of the source in §5. Finally, our conclusion is presented in §6.

2. The Object: *IRAS* 18576+0341

IRAS 18576 was first detected as an IR source by the Survey Program of Infrared Celestial Experiments sensor and the Far-Infrared Sky Survey Experiment telescope (Price, Murdock, & Shivanandan 1981). Their successor program, the Air Force Geophysical Laboratory (AFGL) Infrared Sky Survey (Price & Murdock 1983), confirmed the detection of this IR source and designated the object as AFGL 2298. Infrared Astronomical Satellite (*IRAS*; *IRAS* Explanatory Supplement 1988) also detected it as a point source and assigned the *IRAS* ID (*IRAS* 18576+0341). From its *IRAS* color, *IRAS* 18576 was classified as a region V object (Van der Veen & Habing 1988) and was suspected to be a planetary nebula (PN), which is consistent with the source's very red nature (class H) revealed by the *IRAS* Low Resolution Spectra (LRS; Volk & Cohen 1989; Kwok, Volk, & Bidelman 1997). The LRS also suggested the oxygen-rich (O-rich) nature of this object due to its possible silicate absorption feature at $10\mu m$. García-Lario et al. (1997) obtained near-IR photometric data of the source and classified it as a post-AGB object. However, no optical counterpart has been identified (Hrivnak, Volk, & Kwok (2000) report their unpublished photometry of $V > 23.2$).

Zuckerman & Dyck (1986) were unsuccessful in their search for CO line emission toward

IRAS 18576 with the National Radio Astronomical Observatory (NRAO) 12 m telescope. The authors, nevertheless, classified the object as an oxygen-rich source based on its *IRAS* color. No detection of 22.2 GHz H₂O maser emission was reported in a survey conducted at the Owens Valley Radio Observatory (Zuckerman & Lo 1987). Becker et al. (1994) detected 5 GHz radio continuum emission in the direction of *IRAS* 18576 in their Galactic Plane Survey using the Very Large Array (VLA) and catalogued the source as GRSR5 37.278–0.226. Based on the positional coincidence, they determined the matching probability of the radio source to *IRAS* 18576 to be 98.4% (White, Becker, & Helfand 1991; Becker et al. 1994), suggesting the source to be a PN based on the *IRAS* flux density ratios. In the NRAO VLA Sky Survey (NVSS; Condon, Kaplan, & Terzian 1999), 1.4 GHz radio emission was measured despite the confused background.

Hrivnak, Volk, & Kwok (2000) observed *IRAS* 18576 with the Short Wavelength Spectrometer (SWS; de Graauw et al. 1996) on board the Infrared Space Observatory (*ISO*; Kessler, et al. 1996). The spectrum shows an IR excess peaking near $27\mu\text{m}$ with unidentified IR (UIR) features at 3.3, 6.2, 7.7, 8.6, and $11.3\mu\text{m}$, which are often attributed to polycyclic aromatic hydrocarbons (PAHs; Allamandola, Hudgins, & Sandford 1999 and references therein). The *ISO* detection of carbon-rich (C-rich) material, together with the previous O-rich suggestion by the *IRAS* LRS, makes the source both C/O-rich object. The authors provided several possibilities for the nature of *IRAS* 18576, which include multiple central sources (H II regions or PNs) and a source with multiple shells with differing composition. Table 1 summarizes previous photometric observations of *IRAS* 18576.

3. Observations and Results

3.1. Mid-IR Imaging

We obtained images of *IRAS* 18576 using the University of Arizona/Smithsonian Astrophysical Observatory Mid-IR Array Camera (MIRAC3, Hoffmann et al. 1998), at the NASA Infrared Telescope Facility (IRTF) on 1999 June 7 under photometric conditions. The array is a Boeing HF-16 arsenic-doped silicon blocked-impurity-band hybrid array and has a 128×128 pixel format. The pixel scale was set to $0''.33$ ($42'' \times 42''$ field of view), which ensures a Nyquist sampling of the diffraction-limited PSF of the telescope. The object was observed with 10% ($= \Delta\lambda/\lambda$) bandwidth at 10.3 and $18.0\mu\text{m}$. For flux and point-spread-function (PSF) calibration, we observed α Her (a CGS3 standard; Cohen & Davies 1995) before and after the object to check for variations in the PSF. Measured PSF size (FWHM) was $1''.05 \pm 0''.06$ for $10.3\mu\text{m}$ and $1''.53 \pm 0''.05$ for $18.0\mu\text{m}$. With an east-west telescope nod throw and a north-south secondary chop throw, we mosaiced a final image of size about $25''$ across. Flat-fielding and bad-pixel-masking were applied to sky-subtracted, co-added images before mosaicing. Each individual image was subdivided by 4×4 during mosaicing to make the pixel scale of $0''.0825/\text{pix}$ for accurate registration. The total integration times of the final images are 720 and 400 sec respectively at 10.3 and $18.0\mu\text{m}$, resulting in 1σ rms noise of 14

and 94 mJy arcsec⁻². Absolute flux calibration errors are estimated to be approximately 10%. A full description of the nod-chop procedure, data reduction, and flux calibration processes can be found in Meixner et al. (1999).

Figure 1 shows the reduced images of *IRAS* 18576 at 10.3 and 18.0 μ m. The dust nebula appears roughly circular with about 7'' diameter and there are local emission peaks in the inner region of the nebula. At 10.3 μ m (Figure 1a), three emission peaks are clearly seen and are aligned to form a straight line whose position angle (east from north) is -3.5° . We shall refer to the peaks as northern, central, and southern peaks according to their relative positions. The central peak, located near the geometrical center of the nebula, is unresolved and very likely represents the central star of the system. The northern and southern peaks are 2'' to 2''.5 away from the central peak and more extended than the central peak. The arc-like elongation of the northern and southern peaks seems to encircle the central peak. At 18.0 μ m (Figure 1b), the morphological characteristics are identical to those at 10.3 μ m except that the central peak is less pronounced at 18.0 μ m. The total specific flux of the nebula is 16.7 Jy and 205 Jy respectively at 10.3 and 18.0 μ m: the northern peak accounts for $\sim 70\%$ of the total emission while the rest is shared by the southern peak ($\sim 25\%$) and the central peak ($\sim 5\%$) in both wavebands. Emission from the central peak would impose an upper limit for the direct stellar emission, and we estimated the specific flux from the central star at each wavelength following the iterative method described in Hawkins et al. (1995).

Figure 2 shows the temperature and optical depth maps, which are derived from the source images by following the method described by Dayal et al. (1998). Temperature (Figure 2a) is almost constant over the entire extent of the nebula: 115–135 K with an average of 122 K. There is a single temperature peak coinciding with the central emission peak and temperature falls off as the distance from the central peak increases. This indicates that dust grains in the central peak have higher temperature than dust grains in the surrounding nebula (northern and southern peaks). Thus, it is reasonable to assume that there is a single energy source located in the central emission peak and that the surrounding material is heated by radiation from the central source. This supposition agrees with the behavior of the relative strengths of the emission peaks in the nebula. While the relative emission strength of the northern and southern peaks remains constant, that of the central peak does change at two wavelengths. The observed decrease in the relative emission strength of the central peak at the longer wavelength is a natural consequence at the Rayleigh-Jeans tail of the blackbody curve with high photospheric/dust temperature, whereas the blackbody curve with typical dust grain temperature ($\lesssim 200$ K) generally peaks at mid-IR regions and would not lead to a change in the relative emission strength. The optical depth maps of the dust shell are both similar at 10.3 μ m (Figure 2b) and 18.0 μ m. They indicate that the nebula is optically thin ($\tau_{\text{max}} = 0.058$ and 0.028 respectively at 10.3 and 18.0 μ m) and the northern and southern emission peaks coincide with the regions in which the optical depth is high. This is corroborated by the fact that evidence for the central object can be seen both at 10.3 and 18.0 μ m. Therefore, we interpret the mid-IR morphology of *IRAS* 18576 as limb-brightened edges (northern and southern peaks) of an optically-thin edge-on dust torus surrounding the central star, as seen in, for example, HD

168625 (*IRAS* 18184–1623; Robberto & Herbst 1998; Meixner et al. 1999) and η Car (Polomski et al. 1999). We define the inner radius of the dust torus (r_d) to be $2''.4$, which is the distance from the central star to the northern and southern peaks. In Table 2, we summarize quantities of the CDS in *IRAS* 18576 measured and derived from the mid-IR images.

3.2. Near-IR Photometry

To check the variability of *IRAS* 18576, we obtained *JHK'* photometry of the object with a 40 inch telescope equipped with the Near-Infrared IMager (NIRIM; Meixner, Young Owl, & Leach 1999) at Mt. Laguna Observatory¹ on 1999 June 12 and Nov 14 and 2000 August 5 under clear skies. For flux calibration, we used ELIAS IR standard (Elias et al. 1992) and UKIRT faint IR standard stars (Casali & Hawarden 1992). The standard stars were observed at similar airmasses as the source or at low (~ 1) and high ($\gtrsim 2$) airmasses to perform an airmass correction. Data were taken by shifting the telescope with a 9-point dithering pattern. Each exposure was flat-fielded to eliminate large pixel-to-pixel sensitivity variations in the detector array and was then sky-subtracted before being co-added into a single frame. Flats were created for each waveband by exposing the twilight sky. Sky emission maps were constructed by taking a median of all dithered frames after unusually low and high pixels had been masked out. Our reduction method generally follows the method described in McLean & Teplitz (1996). Table 3 shows *JHK'* photometric data for *IRAS* 18576, in which all magnitudes have been converted to the ELIAS (CIT) magnitudes (Elias et al. 1992) for comparison.

It appears that near-IR brightness of *IRAS* 18576 is in decline in the past decade with the most recent observation (2000 August 5) marking the dimmest ever. Because we did not detect a similar brightness variation in other objects observed on the same nights during the NIRIM observations, we eliminate the possibility of any systematic and/or instrumental effects. Therefore, it is likely that *IRAS* 18576 varies its near-IR brightnesses by a few tenth of a magnitude over a couple of months and about 0.5 magnitudes over a decade.

4. Radiative Transfer Modeling

4.1. 2-D Dust Radiative Transfer

To model IR continuum emission and mid-IR morphologies, we have performed model calculations for an axisymmetric CDS by using a code which solves the radiative transfer equation in a fully two-dimensional grid. This code treats dust absorption, reemission, and (isotropic) scattering

¹Mt. Laguna Observatory is jointly operated by San Diego State University and University of Illinois at Urbana-Champaign.

in an equatorially-enhanced dust distribution (i.e., a presumed radial and latitudinal density variation) with an arbitrary optical depth for a given set of dust species of a single grain size (Meixner et al. 1997; Skinner et al. 1997 for more description of the code). The equatorially-enhanced dust distribution in the model CDS assumes a two-phased mass loss process, in which the central star changes its mode of mass loss from spherically symmetric to axially symmetric with a preferential mass loss towards equatorial directions near the end of the entire mass loss phase. As a result, the pole-to-equator density ratio at the inner shell boundary can be less than unity. The code requires input parameters that can be categorized into three types: stellar, shell, and dust parameters (Table 3). Stellar parameters (the effective temperature, T_{eff} , radius, R_* , and distance) determine the available energy flux for dust heating. Shell parameters (inner and outer shell radii, $r_{\text{d, min}}$ and $r_{\text{d, max}}$, optical depth along the polar direction at some reference wavelength, τ_λ , and other geometrical parameters) specify the dust shell (both physically and morphologically) for radiative transfer calculations. Dust parameters (grain radius and absorption and scattering coefficients, Q_{abs} and Q_{sca}) determine opacity for the shell material.

The use of this dust radiation transfer code is appropriate because direct stellar radiation is estimated to be the dominant heating source for the circumstellar dust grains. The total far-infrared flux (observed specific flux integrated beyond $20\mu\text{m}$) of *IRAS* 18576 is $\sim 3.9 \times 10^{-11} \text{ W}^2 \text{ m}^{-2}$. However, we estimate the amount of far-infrared flux expected from dust grains heated by $\text{Ly } \alpha$ flux (i.e., line emission) to be $\sim 8.7 \times 10^{-13} \text{ W}^2 \text{ m}^{-2}$, following the method described by Zijlstra et al. (1989). Thus, we can safely neglect dust heating due to line emission.

When available, stellar and dust parameters are taken from previous observations in the literature. Otherwise, we determine these parameters through iterative model calculations seeking the best-fit to the spectral energy distribution (SED). Once we achieve the best-fit to the SED, we further iterate calculations with different sets of shell parameters and inclination angle² (θ_{incl}) seeking the best-fit to the SED as well as the mid-IR morphology, which tends to be strongly influenced by the geometric parameters. For example, limb-brightened peaks of a dust torus would not be resolved with a too high inner shell optical depth and a single shell structure can yield different morphologies depending on the inclination angle. The overall shape of the nebula would be ring-like if $\theta_{\text{incl}} \sim 0$ and would be flattened in the direction of the toroidal axis if $\theta_{\text{incl}} \sim 90$. The final best-fit model was achieved, following the guidelines explained above, after ~ 200 model calculations shifting carefully through the parameter space. Because our code does not handle dust stratifications at the moment, the final best-fit model was constructed by combining separate best-fit models for each of the O-rich and C-rich components of the dust shell, assuming the cavity inside the axisymmetric O-rich shell is filled with spherically symmetric C-rich material.

²The inclination angle is the sharp angle between the line of sight and the polar axis.

4.2. Modeling Results

Figure 3 shows the best-fit SED of our model calculations. The best-fit SED (thin solid line) consists of possibly stratified shells of differing composition: the outer O–rich shell (thin dashed line) and the inner C–rich shell (thin dash-dotted line). For comparison, the *ISO* spectrum (thick solid line), the *IRAS* LRS³ (thick dashed line), and other photometric data (symbols) are shown. Table 3 lists input and derived quantities for the best-fit model.

We also show the best-fit synthesized images at 10.3 and 18.0 μm (Figure 4). The final synthesized images were constructed by adding the observed standard star images to the O–rich shell model images because the code does not produce images with a resolved central star. The model images were convolved with a Gaussian profile whose FWHM is equal to the observed FWHM at each waveband before the central star was added. The two emission peaks arise from equatorially-enhanced (the pole-to-equator density ratio = 0.5) O–rich dust distribution viewed with 45° inclination angle. The resulting morphologies are very sensitive to the inclination angle when the shell is optically thin and would completely be altered if the inclination angle is changed by $\sim 10\%$. The axis of the dust torus is rotated in the plane of the sky at a position angle of 86.5° East of North and the near side of the dust torus is to the east from the center. The slight asymmetry seen in the shape of each emission peak is due to self-extinction arising from the polar density variation.

5. Discussions

5.1. The Central Star and its Distance

Because we have no prior knowledge about the central star, we must iteratively derive T_{eff} and R_* from radiative transfer calculations. Consider an optically thin, isothermal (at T_d) dust shell. When dust grains of a uniform grain size are in thermal equilibrium with the ambient stellar radiation field, we can relate the luminosity of the star (L_*), shell radius (r_d), and dust temperature by equating the rate of energy absorption and reemission as

$$T_d \propto \left(\frac{L_*}{r_d^2} \right)^{\frac{1}{n+4}}. \quad (1)$$

Here, we have assumed a power-law dust grain emissivity ($Q_{\text{abs}} \propto \nu^n$) and the constant of proportionality is solely determined by the dust grain properties. Because both L_* and r_d are observable quantities modulo distance, we can eliminate the distance dependence in eq.(1) and rewrite it as

$$T_d \propto \left(\frac{F_*}{r_d^2} \right)^{\frac{1}{n+4}}, \quad (2)$$

³*IRAS* LRS spectrum does not have an absolute flux calibration and is shown primarily to show the shape. The best-fit was determined by comparing model fluxes with the *ISO* spectrum and other photometric data.

in which F_* is the flux of the source and r'_d is the angular radius of the dust shell in arcsec. The dust temperature effectively defines the location of the IR excess peak in the SED. Therefore, eq.(2) indicates that we can fix F_* by fitting the IR peak location (i.e., T_d) by iterating on F_* and dust species in radiative transfer calculations because r'_d is observationally determined. It is also possible to constrain F_* by using the observed IR flux of the source (F_*^{obs}). Photometric data obtained by *ISO* (Hrivnak, Volk, & Kwok 2000) and other near-IR observations (García-Lario et al. 1997) yielded $F_*^{\text{obs}} \sim 2.3 \times 10^{-7} \text{ erg s}^{-1} \text{ cm}^{-2}$. The near-IR part of the *ISO* spectrum (Hrivnak, Volk, & Kwok 2000) suggests the presence of PAHs. However, solely C-rich models yielded a warmer dust temperature than can be produced by the detached dust shell of $2''.4$ angular radius due to generally higher opacity of carbonaceous material. Models with a mixture of amorphous carbon and astronomical silicates produced too high dust temperature as well. Our iterative calculations concluded that $F_* \sim 4 \times F_*^{\text{obs}}$ with astronomical silicates would produce the best-fit mid-IR SED to observations. This means that the O-rich dust shell processes about 25% of the stellar flux, and it is consistent with our finding that the dust shell of *IRAS* 18576 is optically thin.

To recover T_{eff} and R_* from the derived F_* , we need to determine the distance to *IRAS* 18576. Previous CO observations do not provide any kinematic information of the source (Zuckerman & Dyck 1986) probably because of the confused background reported by Condon, Kaplan, & Terzian (1999). Recent CO observations failed to obtain any reliable kinematic data due to the lack of clear background in the crowded radio field around *IRAS* 18576 (D. Fong 1999, priv. comm.). Therefore, we estimated the distance to *IRAS* 18576 by determining the total visual extinction (A_V) that is required to make our model near-IR SED fit the observed one. The near-IR colors of *IRAS* 18576 are very red. Because the dust shell is assumed to process only about 25% of the stellar radiation, it is reasonable to explain the red near-IR colors by a severe interstellar extinction. Our best fit model indicated that A_V would have to be about 28 to account for the extinction assuming a typical total-to-selective extinction ratio (R_V) of 3.1. Such a high A_V value may not be surprising because of the Galactic coordinates of *IRAS* 18576, $(l, b) = (37.3^\circ, -0.3^\circ)$: the line of sight lies in the Galactic plane grazing the outskirts of the bulge. According to the full-sky dust maps compiled from *COBE/DIRBE* and *IRAS* maps (Schlegel, Finkbeiner, & Davis 1998), the Galactic selective extinction, $E(B-V)$, along the line of sight to *IRAS* 18576 is estimated to be 18.25, which equals to the Galactic total visual extinction of 56.58. If we assume the Parenago type exponential distance scaling of A_V (Parenago 1940), $A_V \sim 28$ can be achieved if *IRAS* 18576 is located around 10 kpc away. This estimate is uncertain because the assumed distance scaling law of A_V does not account for local clumping of reddening material and may locally have a drastically different form.

Alternatively, the distance to *IRAS* 18576 can be estimated by iteratively searching for a high enough L_* to heat the optically thin dust shell of *IRAS* 18576 (Figure 2b) to the observed temperature ($T_d = 115 - 135 \text{ K}$) because the distance directly scales the luminosity of the object. The optical depth maps have yielded very low τ values ($\tau_{\text{max}} = 0.058$ and 0.028 at 10.3 and $18.0 \mu\text{m}$, respectively). With these optical depth, *IRAS* 18576 would have to be located about 25 kpc, which yields an unrealistically high luminosity for a star and brings the object close to the

edge of the Galaxy in the direction of the object. Thus, we kept increasing the optical depth of the dust shell until the toroidal structure would be unresolved while iteratively adjusting the distance. After further iteration, we concluded that 10 ± 3 kpc would scale L_* high enough so that model calculations would yield the dust peak in the observed SED, using the highest optical depth possible to reproduce the resolved dust toroidal structure in our models (Table 3 and Figure 4). Considering the above two independent means to estimate the distance, we adopted 10 kpc to be the distance to *IRAS* 18576 because there is no alternate source of data. With the adopted distance of 10 kpc, L_* is 1.1×10^{40} ergs s $^{-1}$ ($= 10^{6.4} L_\odot$).

We can then constrain T_{eff} from the position of the redward slope of the stellar emission peak with respect to the observed SED. A lower T_{eff} would shift the stellar peak to the red and would effectively increase the stellar emission in the wavelengths of our interest while leaving the dust peak virtually unchanged. Thus, the lower limit for T_{eff} can be obtained because any lower T_{eff} than the limit would yield too much stellar flux than observed. We used the $10.3\mu\text{m}$ emission in constraining T_{eff} because this wavelength range seemed to retain the most pristine stellar emission characteristic free from extinction and/or dust feature emission. Further iteration yielded the lower T_{eff} limit of ~ 9000 K, which corresponds to the upper R_* limit of $\sim 700R_\odot$. However, it is more difficult to constrain the upper T_{eff} limit defining the possible range for T_{eff} because the emission properties in the optical to near-IR depend more heavily on the distance to the object (i.e., A_V) and the location of the C-rich shell that is considered to be situated inside the O-rich dust shell (see below). Nevertheless, iterative calculations suggested that $T_{\text{eff}} \sim 15000 \pm 6000$ K would be a likely range of the effective temperature. The model calculations with this T_{eff} range requires $A_V = 24 \sim 32$ to be consistent with the observed data.

5.2. Dust Shell Composition and Structure

The presence of silicates in *IRAS* 18576 was originally suspected from the apparent absorption feature at $10\mu\text{m}$ (Zuckerman & Dyck 1986; Volk & Cohen 1989) seen in the LRS. This $10\mu\text{m}$ dip, however, is a false depression caused by the strong neighboring PAH features at 8.6 and $11.3\mu\text{m}$, because the CDS is observed to be optically thin enough that the central star is visible even at the mid-IR (Figure 1). This makes it difficult to identify the silicate species from the shape of the $9 - 11\mu\text{m}$ silicate features (Speck 1998 and references therein). The featureless far-IR portion of the spectrum also makes it difficult to determine if there exists a particular crystalline silicate species. Therefore, we used optical constants for astronomical silicates (Laor & Draine 1993) which empirically simulate a mixture of different types of silicates. With iteratively obtained $F_* \sim 4 \times F_*^{\text{obs}}$, the model SED fits the overall shape of the *ISO* SED very well at the long wavelength regions ($\gtrsim 18\mu\text{m}$) and at the $10\mu\text{m}$ trough (Figure 3, thin dashed lines).

The model SED arising only from the O-rich shell shows emission “deficits” in the near-IR ($\lesssim 10\mu\text{m}$) and at the blueward shoulder of the IR peak ($10 - 18\mu\text{m}$). To account for the presence of the observed C-rich material, we considered an inner C-rich (PAHs) region, which is surrounded

by the O–rich shell of angular radius $2''.4$. C–rich material is expected to be closer to the central star because of the presumed ionization state of PAHs: the comparable strengths of 7.7 and $11.2\ \mu\text{m}$ emission peaks suggest that PAHs are marginally ionized (Molster et al. 1996). The inner C–rich shell adequately compensates the emission deficits (Figure 3, thin dot-dashed lines). The C–rich shell does not reproduce each emission line of the UIR features because we have used optical constants of amorphous carbon grains of $0.002\ \mu\text{m}$ to substitute for the yet unavailable optical constants of PAHs. This dust grain size is comparable to the major PAH cluster size of 300 – 400 C–atoms (Omont 1986) whose presence is typically observed through 5 – $10\ \mu\text{m}$ and 11 – $15\ \mu\text{m}$ emission plateaus (Beintema et al. 1996). Due to lack of spatial information in the near-IR, we determined the inner C–rich shell radius through model iterations.

The deficit at the longer wavelengths (15 – $20\ \mu\text{m}$), on the other hand, seems to be excessive because very little PAH emission is expected in this wavelength region. To boost IR emission from 15 to $20\ \mu\text{m}$, we included amorphous aluminum oxide (Al_2O_3), whose Q_{abs} has a local maximum around $13\ \mu\text{m}$, according to the mass abundance ratio consistent with the cosmic abundance ($\sim 96\%$ amorphous silicates and $\sim 4\%$ aluminum oxides). The inclusion of aluminum oxide grains is not entirely *ad hoc*; they are considered to be the nucleation cores in the heterogeneous dust nucleation theory (Speck 1998 and references therein) and the *ISO* spectrum shows a number of possible narrow peaks in the 11 – $13\ \mu\text{m}$ plateau (especially 11.9 and $12.8\ \mu\text{m}$), which may be due to aluminum oxides (Begemann et al. 1997). Although we did not attempt model calculations with any specific silicate species, the presence of an emission plateau near $34\ \mu\text{m}$, which our model SED fails to reproduce (due to the use of amorphous silicates), suggests the presence of crystalline olivines (forsterites), which have an emission peak in that region.

Our best-fit model agrees with the general behavior of the observed SED with the $10\ \mu\text{m}$ trough adequately reproduced. This method obviously does not conserve flux at the interface between the two shells in the sense that the O–rich shell receives stellar flux which should have been reduced by the presence of the C–rich shell. However, the very optically thin C–rich shell is estimated to require only about 0.5% of the total flux of the central star. Therefore, considering that the O–rich shell itself processes only $\sim 25\%$ of the total stellar flux, we conclude that our results would still hold even if calculations were done in a strictly flux conserving manner.

5.3. Nature of IRAS 18576+0341

The derived stellar parameters put the star above the empirical luminosity limit (Humphreys-Davidson limit; Humphreys & Davidson 1979) in the Hertzsprung-Russell diagram. *IRAS* 18576 would then likely be a luminous blue variable (LBV) or a red super giant (RSG). The derived luminosity of *IRAS* 18576 is unusually high ($L_* = 10^{6.4} L_\odot$) for a RSG, however, there exist LBVs whose L_* is comparable to that of *IRAS* 18576 (e.g., η Car and AG Car, Humphreys & Davidson 1994 and references therein). Although the expected temperature range for the object is rather low ($T_{\text{eff}} = 15000 \pm 6000\ \text{K}$) for a typical LBV, it is still higher than that of the coolest LBVs. The

fact that T_{eff} would not be lower than 9000 K seems to favor the LBV interpretation. One of the coolest LBV candidates, HD 168625, was found to have T_{eff} in the range of 12000 – 15000 K (Nota et al. 1996). Interestingly, this cool LBV is also found to be associated with an extended dust shell with the equatorial enhancement (Robberto & Herbst 1998; Meixner et al. 1999).

There are a number of observational similarities between *IRAS* 18576 and other LBVs. The mid-IR morphology of LBVs is characterized especially by their signature limb-brightened lobes with a separate central source (e.g., η Car, Polomski et al. 1999; AG Car, Trams, Waters, & Voors 1996; HD 168625, Robberto & Herbst 1998; Meixner et al. 1999), which are very similar to what we have seen in *IRAS* 18576 (Figure 1). Morphologically, it is very likely that the central emission peak represents the one and only energy source in the system and illuminates the surrounding lobes. The limb-brightened lobes strongly suggest the presence of an equatorially enhanced dust distribution in the CDS, and it is consistent with what our model calculations assume. This axisymmetric geometry has been thought to be a common signature of the LBV nebulae caused by a sharp pole-to-equator density contrast (Nota et al. 1995). Although the origin of the equatorial enhancement is not yet fully understood, a number of possible mechanisms have been suggested. For example, Langer, García-Segura, & Mac Low (1999) considered rotating stars near their Eddington limit and showed hydrodynamically that highly non-spherical mass loss would occur. On the other hand, Damineli et al. (2000) have spectroscopically confirmed the binarity of η Car, and it has also been hydrodynamically shown that such binary systems can generate an equatorially-enhanced material distribution around the central system in the context of the PN formation (Mastrodemos & Morris 1999). Whatever the true scenario may be, the observed limb-brightened mid-IR lobes clearly showed the non-sphericity of the system, and any dynamical models should be able to reproduce such geometry.

Spectral characteristics of *IRAS* 18576 are also similar to those of other LBVs. Large IR excesses due to dust grains have been observed in LBVs, and the observed mid-IR flux levels of *IRAS* 18576 are comparable to other LBVs: it is approximately a few times brighter than typical LBVs (Lamers et al. 1996) but a couple of orders of magnitudes dimmer than η Car (Morris et al. 1999). Both amorphous and crystalline silicates have been identified in the LBV dust shells (Waters et al. 1997). The presence of C-rich material in a dominantly O-rich shell has already been seen in other LBVs (e.g., Voors et al. 1999). Moreover, *IRAS* 18576 seems to be varying its brightness with the timescale (months to years) and the widths of magnitude (about 0.1 – 0.5) consistent with what have been observed in LBVs.

The observed and derived physical quantities of the dust shell are also consistent with LBV characteristics. The maximum extent of the observed mid-IR dust nebula ($\gtrsim 5\sigma$ detection) is about $10''$, which equals to ~ 0.5 pc at 10 kpc. Considering the fact that the mid-IR observations probe only the innermost regions of the dust shell, this value is reasonable for the inner radius of a typical LBV nebula (e.g., Nota et al. 1995; Chu, Weis, & Garnett 1999). The total dust mass in the *IRAS* 18576 dust torus is estimated to be $\sim 0.1M_{\odot}$. This estimate depends on the outer radius of the dust torus, which is assumed to be 6 times larger than the inner radius. The estimated dust mass

is nearly a factor of 10 higher than typical LBV dust mass quantities (Nota et al. 1995) but is comparable to the estimated dust mass of a similar temperature (100 ± 10 K) component in η Car (Morris et al. 1999). The total mass lost by the star and the rate of mass loss are estimated to be about $75M_{\odot}$ and $6.8 \times 10^{-6}M_{\odot} \text{ yr}^{-1}$ using the canonical gas-to-dust ratio of 100 and an assumed expansion velocity of 50 km s^{-1} (e.g., Nota et al. 1995). Both of these values depend on the outer radius of the entire mass loss shell, which is not constrained by observations and is assumed to be 50 times as the inner shell radius.

Based on the mid-IR morphology and IR photometric and spectroscopic characteristics, and results from radiative transfer calculations, *IRAS* 18576 is likely a very luminous star surrounded by an optically thin, possibly stratified C/O–rich dust shell located at about 10 kpc in the direction in which very severe interstellar extinction can occur. Physical parameters of the *IRAS* 18576 system derived from radiative transfer calculations suggest that *IRAS* 18576 is probably a LBV candidate. This conclusion derived from the fact that the derived luminosity for *IRAS* 18576 was so high and that other evidence seemed to be consistent with our conclusion. However, given the uncertainties involved in the distance determination, it is also possible that *IRAS* 18576 is a RSG. Therefore, it is necessary to observationally uncover the physical characteristics of the central star to determine the exact evolutionary status of *IRAS* 18576. Because *IRAS* 18576 is not visible in the optical due to heavy extinction, we need near-IR spectroscopic information to constrain the physical parameters of the central star. We also need to continue obtaining near-IR photometry to better characterize the variability of the source. We are planning such follow-up observations.

Regardless of the exact evolutionary status, *IRAS* 18576 seems highly likely to be an evolved, massive post-main-sequence star. The axisymmetry of the circumstellar shells of evolved massive stars has long been indirectly suggested from the strongly non-spherical shapes of optical nebulosities associated with LBVs (e.g., Nota et al. 1995 and references therein). Our discovery of the dust shell around *IRAS* 18576 is one of the few direct evidence for the equatorial density enhancement in the circumstellar environment of massive post-main-sequence stars (e.g., η Car, Polonski et al. 1999; AG Car, Trams, Waters, & Voors 1996; HD 168625, Robberto & Herbst 1998; Meixner et al. 1999). For low to intermediate mass stars, it is well established that the mode of mass loss is highly axisymmetric (e.g., Ueta, Meixner, & Bobrowsky 2000). It now appears that an axisymmetric mass loss also operates for massive stars, and therefore, stellar wind scenarios for massive stars would be able to produce the observed pole-to-equator density contrast and generate axisymmetric CDSs.

6. Conclusions

We have discovered an extended mid-IR emission around *IRAS* 18576 and presented the mid-IR images at 10.3 and 18.0 μm . The two emission peaks, which are concentrically elongated and symmetrically oriented on the opposite sides of the central peak, are typically the results from an optically thin, limb-brightened edges of the dust torus viewed rather edge-on. We also present

new near-IR photometry of the object which demonstrates its variability. Although the source lies in the region of the sky in which a severe Galactic extinction has been observed, we have constructed a model using all of the available information. The derived physical quantities for the central star and dust shell and variability of the object suggest that *IRAS* 18576 is a possible LBV candidate with $L_* = 10^{6.4} L_\odot$ and $T_{\text{eff}} = 15000 \pm 9000$ K. The uncertainties involved in the distance determination leave possibilities that the object could be a RSG, and further observational work is needed to determine the exact evolutionary state of the star. While the main dust shell is composed of silicate dust grains, an additional C-rich (composed of PAHs) shell likely exists inside of the O-rich shell. The axisymmetric nature of the dust toroid is characterized by the calculated pole-to-equator density ratio of 0.5. While the origin of the equatorial enhancement is still open for further discussion, the axisymmetry seems to be a common feature in mass loss from massive stars as in the case for low to intermediate stars.

Ueta and Meixner are supported by NSF CAREER Award AST-9733697. We would like to thank A. K. Speck for enlightening discussions on dust properties, B. J. Hrivnak, K. Volk, and S. Kwok for providing their ISO spectra, and D. Fong for performing the CO observation. We are also grateful to an anonymous referee for many useful comments and suggestions. This research has made use of the Jena - St. Petersburg Database of Optical Constants (JPDOC; <http://www.astro.uni-jena.de/Users/database/f-dbase.html>) operated by the Astrophysical Institute of the Friedrich Schiller University, Jena, Germany, and the Astronomical Institute of the St. Petersburg University, Russia, and the SIMBAD database, operated at Centre de Données astronomiques, Strasbourg, France.

REFERENCES

- Allamandola, L. J., Hudgins, D. M., & Sandford, S. A. 1999, *ApJ*, 511, L115
- Becker, R. H., White, R. L., Helfand D. J., & Zoonematkermani, S. 1994, *ApJS*, 91, 347
- Begemann, B., Dorschner, J., Henning, TH., Mutschke, H., Gürtler, J., Kömpe, C., & Nass, R. 1997, *ApJ*, 476, 199
- Beintema, D. A., van den Ancker, M. E., Molster, F. J., Waters, L. B. F. M., Tielens, A. G. G. M., Waelkens, C., de Jong, T., de Graauw, Th., Justtanont, K., Yamamura, I., Heras, A., Lahuis, F., & Salama, A. 1996, *A&A*, 315, L369
- Casali, M. M. & Hawarden, T. G. 1992, *JCMT UKIRT Newsletter*, 4, 33
- Chu, Y.-H., Weis, K., & Garnett, D. R. 1999, *AJ*, 117, 1433
- Cohen, M. & Davies J. K. 1995, *MNRAS*, 276, 715
- Condon, J. J., Kaplan, D. L., & Terzian, Y. 1999, *ApJS*, 123, 219

- Damineli, A., Kaufer, A., Wolf, B., Stahl, O., Lopes, D. F., & de Araújo, F. X. 2000, *ApJ*, 528, L101
- Dayal, A., Hoffmann, W. F., Bieging, J. H., Hora, J. L., Deutsch, L. K., & Fazio, G. G. 1998, *ApJ*, 492, 603
- de Graauw, T. et al. 1996, *A&A*, 315, L49
- Egan, M. P., Price, S. D., Moshir, M. M., Cohen, M., Tedesco, E. F., Murdock, T. L., Zweill, A., Burdick, S., Bonito, N., Gugliotti, G. M., & Duszlak, J. 1999, The Midcourse Space Experiment Point Source Catalog, Version 1.2 Explanatory Guide, Air Force Research Laboratory Technical Report, AFRL-VS-TR-1999-1522
- Elias, J. H., Frogel, J. A., Matthews, K., & Neugebauer, G. 1982, *AJ*, 87, 1029
- García-Lario, P., Manchado, A., Pych, W., Pottasch, S. R. 1997, *A&AS*, 126, 479
- Harman, A., K., Ninomiya, S., & Adachi, S. 1994, *J. Appl. Phys.*, 76, 8032
- Hawkins, G. W., Skinner, C. J., Meixner, M., Jernigan, J. G., Arens, J. F., Keto, E., & Graham, J. R. 1995, *ApJ*, 452, 314
- Hoffmann, W. F., Hora, J. L., Fazio, G. G., Deutsch, L. K. & Dayal, A. 1998, in *Infrared Astronomical Instrumentation*, ed. A. M. Fowler, *Proc. SPIE* 3354, 647, 658
- Hrivnak, B. J., Volk, K., & Kwok, S. 2000, *ApJ*, 535, 275
- Humphreys, R. M. & Davidson, K. 1994, *ApJ*, 232, 409
- Humphreys, R. M. & Davidson, K. 1994, *PASP*, 106, 1025
- Joint IRAS Science Working Group 1988, *Infrared Astronomical Satellite Catalogs and Atlases*, Version 2. Explanatory Supplement, eds. C. A. Beichmen, G. Neugebauer, H. J. Habing, P. E. Clegg, & T. J. Chester (Washington, DC: NASA Reference Publication)
- Kessler, M. F., Steinz, J. A., Anderegg, M. E., Clavel, J., Drechsel, G., Estaria, P., Faelker, J., Riedinger, J. R., Robson, A., Taylor, B. G., & Ximenez de Ferran, S. 1996, *A&A*, 315, L27
- Kwok, S., Volk, K., & Bidelman, W. 1997, *ApJS*, 112, 557
- Lamers, H. J. G. L. M., Morris, P. W., Voors, R. H. M., van Gent, J. I., Waters, L. B. F. M., de Graauw, Th., Kudritzki, R. P., Najarro, F., Salama, A., & Heras, A. M. 1996, *A&A*, 315, L225
- Langer, N., García-Segura, G., & Mac Low, M.-M. 1999, *ApJ*, 520, L49
- Laor, A. & Draine, B. T. 1993, *ApJ*, 402, 441

- Mastrodemos, N. & Morris, M. 1999, *ApJ*, 523, 357
- McLean, I. S. & Teplitz, H. 1996, *AJ*, 112, 2500
- Meixner, M., Skinner, C. J., Graham, J. R., Keto, E., Jernigan, J. G., & Arens, J. F. 1997, *ApJ*, 482, 897
- Meixner, M., Ueta, T., Dayal, A., Hora, J. H., Fazio, G., Hrivnak, B. J., Skinner, C. J., Hoffman, W. F., & Deutsch, L. K. 1999, *ApJS*, 122, 221
- Meixner, M., Young Owl, L., & Leach, R. 1999, *PASP*, 111, 997
- Molster, F. J., van den Ancker, M. E., Tielens, A. G. G. M., Waters, L. B. F. M., Beintema, D. A., Waelkens, C., de Jong, T., de Graauw, Th., Justtanont, K., Yamamura, I., Vandenbussche, B., & Heras, A. 1996, *A&A*, 315, L373
- Morris, P. W., Waters, L. B. F. M., Barlow, M. J., Lim, T., de Koter, A., Voors, R. H. M., Cox, P., de Graauw, Th., Henning, Th., Hony, S., Lamers, H. J. G. L. M., Mutschke, H., & Trams, N. R. 1999, *Nature*, 402, 502
- Nota, A., Livio, M., Clampin, M., Schlte-Landbeck, R. 1995, *ApJ*, 448, 788
- Nota, A., Pasquali, A., Clampin, M., Pollacco, D., & Scuderi, S. 1996, *ApJ*, 473, 946
- Omont, A. 1986, *A&A*, 164, 159
- Parenago, P. P. 1940, *Astron. Zhur.*, 17, 3
- Polonski, E. F., Telesco, C. M., Pia, R. K., & Fisher, R. S. 1999, *AJ*, 118, 2369
- Price, S. D. & Murdock, T. L. 1983, *The Revised AFGL Infrared Sky Survey Catalog*, AFGL-TR-83-0161 (Hanscom AFB, MA: Air Force Geophysics Laboratory, Air Force Systems Command, USAF)
- Price, S. D., Murdock, T. L. & Shivanandan, K. 1981, in *Infrared astronomy - Scientific/military thrusts and instrumentation*, ed. Howard J. Stears & Nancy W. Boggess, *SPIE*, 280. 33
- Robberto, M., & Herbst, T. M. 1998, *ApJ*, 498, 400
- Schlegel, D. J., Finkbeiner, D. P. & Davis, M. 1998, *ApJ*, 500, 525
- Skinner, C. J., Meixner, M., Barlow, M. J., Collison, A. J., Justtanont, K., Blanco, P., Pina, R., Ball, J. R., Keto, E., Arens, J. F., & Jernigan, J. G. 1997, *A&A*, 3328, 290
- Speck, A. K. 1998, *PhD Thesis*, University College London
- Trams, N. R., Waters, L. B. F. M., & Voors, R. H. M. 1996, *A&A*, 315, L213
- Ueta, T., Meixner, M., & Bobrowsky, M. 2000, *ApJ*, 528, 861

- Van der Veen, W. E. C. J. & Habing, H. J. 1988, A&A, 194, 125
- Volk, K. & Cohen, M. 1989, AJ, 98, 931
- Voors, R. H. M., Waters, L. B. F. M., Morris, P. W., Trams, N. R., de Koter, A. & Bouwman, J. 1999, 341, L67
- Waters, L. B. F. M., Morris, P. W., Voors, R. H. M., & Lamers, H. J. G. L. M. 1997, in Luminous Blue Variables: Massive Stars in Transition eds. A. Nota & H. J. G. L. M. Lamers, ASP Conferenc Series, 120, 326
- White, R. L., Becker, R. H., & Helfand D. J. 1991, ApJ, 371, 148
- Zijlstra, A. A., te Lintel Hekkert, P., Pottasch, S. R., Caswell, J. L., Ratag, M., & Habing, H. J. 1989, A&A, 217, 157
- Zubko, V. G., Mennella, V., Colangeli, L., & Bussoletti, E. 1993, MNRAS, 282, 1321
- Zuckerman, B. & Dyck, H. M. 1986, ApJ, 311, 345
- Zuckerman, B. & Lo, K. Y. 1987, A&A, 173, 263

Fig. 1.— Observed grayscale images of *IRAS* 18576+0341 at $10.3\mu m$ (a; top) and $18.0\mu m$ (b; bottom) with north being up and east being to the left. The tick marks show relative offsets in arcseconds. Contours are spaced by 10% of the peak intensity and their colors are inverted for the ease of viewing. The lowest contour is equivalent of 4.3σ and 6.7σ level of emission respectively at 10.3 and $18.0\mu m$. Local peak intensities are, from northern to southern peak, 0.57 , 0.49 , and 0.38 Jy arcsec $^{-2}$ at $10.3\mu m$ and 6.3 , 3.9 , and 4.4 Jy arcsec $^{-2}$ at $18.0\mu m$. The PSF size (FWHM) is indicated by a black circle in each frame at the lower left: $1''.05$ at $10.3\mu m$ and $1''.53$ at $18.0\mu m$.

Fig. 2.— Temperature map (a; top) and optical depth map at $10.3\mu m$ (b; bottom) of *IRAS* 18576 following the display convention of Figure 1. (a) Temperature contours go from 135 to 115 K with an interval of 2.5 K. The spurious peaks around the nebula are artifacts occurred during the derivation. (b) Optical depth contour interval is 10% of the peak value, 0.058 .

Fig. 3.— The spectral energy distribution of the best-fit model (9000 K, $700R_*$, 10 kpc): thin solid, dashed, and dot-dashed lines respectively show the total SED, contribution from the O-rich shell, and contribution from the C-rich shell with ISM extinction (bottom lines) and without extinction (top lines). Observational data are indicated by thick lines (solid – *ISO*; Hrivnak et al. 2000, dashed – *IRAS* LRS; Volk and Cohen 1989) and symbols (circles – *IRAS* photometry; *IRAS* Explanatory Supplement 1988, asterisks – AFGL photometry; Price & Murdock 1983, crosses – near-IR photometry; García-Lario et al. 1997, stars – MSX photometry; Egan et al. 1999, squares; this observation).

Fig. 4.— Model Images of *IRAS* 18576+0341 at $10.3\mu m$ (a; top) and $18.0\mu m$ (b; bottom) following the display convention of Figure 1. Contours are spaced by 10% of the peak intensity. Peak intensities are 0.40 Jy arcsec $^{-2}$ (at $10.3\mu m$) and 8.3 Jy arcsec $^{-2}$ (at $18.0\mu m$). The central star (the observed PSF) was scaled to reflect the observed northern-to-central peak ratio at each wavelength.

Table 1. Previously Obtained Photometry on *IRAS* 18576+0341

RA (2000)	DEC (2000)	11.0 μm^a (Jy)	12.0 μm^b (Jy)	19.8 μm^a (Jy)	25.0 μm^b (Jy)	27.4 μm^a (Jy)	60.0 μm^b (Jy)	100.0 μm^b (Jy)	5 GHz ^c (mJy)	1.4 GHz ^d (mJy)
19:00:11.2	+03:45:46	81.4	58.48	356.9	424.2	649.4	274.5	< 1661	78.1	8.1 \pm 0.7

References. — a: AFGL survey (Price & Murdock 1983), b: *IRAS* (*IRAS* Explanatory Supplement 1988), c: GPS survey (Becker et al. 1994), d: NVSS survey (Condon, Kaplan, & Terzian 1999)

Note. — See Table 4 for the near-infrared photometric data and Figure 3 for *IRAS* LRS and *ISO* spectra. *IRAS* 100.0 μm data is an upper limit.

Table 2. Measured and Derived Quantities of the Dust Shell around *IRAS* 18576+0341

Quantity	10.3 μm	18.0 μm
Flux Density (Jy)	16.7	205
Diameter (FWHM)	6''.2	6''.9
Toroidal Shell Radius	2''.4	
Dust Temperature	115 \sim 135 K	
Optical Depth	\lesssim 0.058	\lesssim 0.028

Table 3. Input and Derived Model Quantities

Stellar Parameters		
L_*	$10^{6.4} L_\odot$	
T_{eff}	$15000 \pm 6000 \text{ K}$	
R_*	$120 - 700 R_\odot$	
d	$10 \pm 3 \text{ kpc}$	
ISM A_V	$24 - 32$	
Dust Shell Parameters		
	O-rich Shell	C-rich Shell
$r_{\text{d, min}} \text{ (pc)}$	0.12	0.0038
$r_{\text{d, max}} \text{ (pc)}$	5.8	0.12
θ_{incl}	$45 \pm 5^\circ$	
$T_{\text{d}} \text{ at } r_{\text{d, min}} \text{ (K)}$	112	512
$\tau_{10.3\mu\text{m}, \text{ eq}}$	0.54	0.036
$\tau_{10.3\mu\text{m}, \text{ pole}}$	0.15	0.036
$\rho_{\text{pole}}/\rho_{\text{eq}} \text{ at } r_{\text{d, min}}$	0.5	1
$\dot{M}_{\text{dust}} \text{ (} M_\odot/\text{yr)}$	6.8×10^{-6}	5.7×10^{-9}
$v_{\text{exp}}^{\text{a}}$	50 km s^{-1}	50 km s^{-1}
$\tau_{\text{dyn}} \text{ (yr)}^{\text{b}}$	1.1×10^5	2×10^3
a	$0.01 \mu\text{m}$	$0.002 \mu\text{m}$
Composition ^c	96% Amorphous Silicates 4% Alminum Oxides	100% Amorphous Carbon

^aTypical v_{exp} for LBVs (e.g., Nota et al. 1995).

^b $\tau_{\text{dyn}} = r_{\text{d}}/v_{\text{exp}}$

^cAbundance % by mass; References: amorphous silicates; Laor & Draine (1993), aluminum oxides; Begemann et al. (1997); Harman, Ninomiya, & Adachi (1994), amorphous carbon; Zubko et al. (1996).

Table 4. *JHK'* Photometry of *IRAS* 18576+0341

Date	<i>J</i>	<i>H</i>	<i>K'</i>	Ref.
1989 May–Jun	12.0 ±0.3	8.99±0.03	6.91±0.02	1
1999 Jun 12	12.21±0.12	8.94±0.06	7.07±0.05	2
1999 Nov 14	12.44±0.07	9.32±0.05	7.60±0.08	2
2000 Aug 5	12.61±0.51	10.44±0.16	8.58±0.11	2

References. — 1. García-Lario et al. (1997), 2. NIRIM observations.

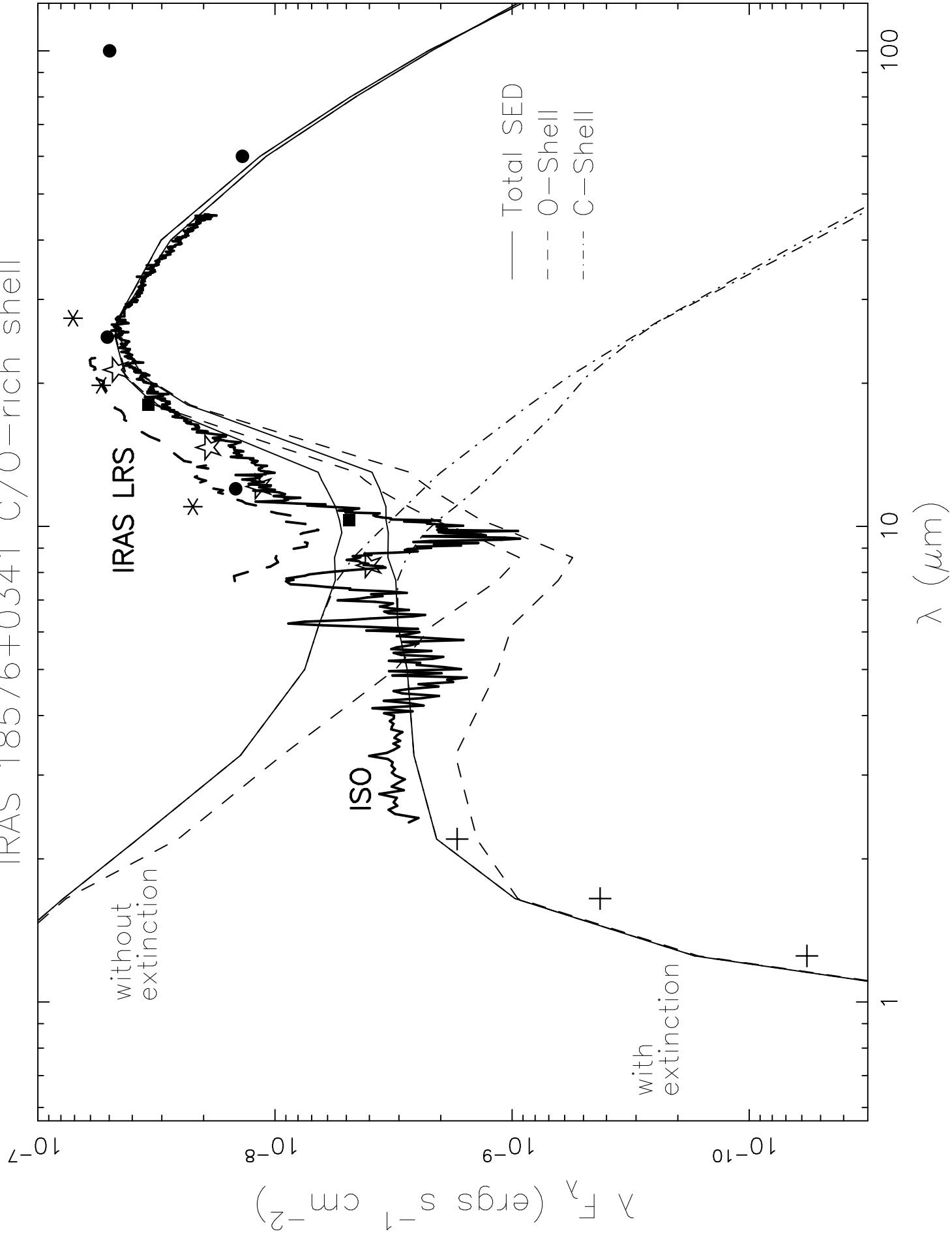
This figure "fig1.jpg" is available in "jpg" format from:

<http://arxiv.org/ps/astro-ph/0010099v1>

This figure "fig2.jpg" is available in "jpg" format from:

<http://arxiv.org/ps/astro-ph/0010099v1>

IRAS 18576+0341 C/O-rich shell



This figure "fig4.jpg" is available in "jpg" format from:

<http://arxiv.org/ps/astro-ph/0010099v1>